Energy Engineering

Tech Science Press

Doi:10.32604/ee.2025.072397

ARTICLE

Improved Three-Vector Model Predictive Current Control Strategy for Fixed Switching Frequency on a Grid-Connected Inverter

Hongsheng Su, Dan Li* and Yuwei Du

School of Automation and Electrical Engineering, Lanzhou Jiaotong University, Lanzhou, 730070, China

*Corresponding Author: Dan Li. Email: 12231623@stu.lzjtu.edu.cn

Received: 26 August 2025; Accepted: 11 November 2025; Published: 27 April 2026

ABSTRACT: When the three-phase grid-connected inverter system is in operation, there are problems of significant switching losses and power losses. At the same time, if the switching frequency is not fixed, it will lead to problems such as a high content of low-order harmonics in the current on the grid side. This paper takes the three-phase grid-connected inverter as the research object and proposes a solution. Establish a mathematical model for the inverter system and analyze the transformation relationships of relevant electrical quantities across different coordinate systems. First, the paper proposes an improved three-vector model predictive current control algorithm. It employs an orthogonal-axis current zero-crossing method to calculate vector action times, enabling rapid and efficient determination of the desired sector. Then, based on this, an optimized switching sequence method is proposed. It fixes the switching frequency by adding a constraint term to the objective function. Finally, the effectiveness of the proposed method was validated through simulation and experimental results. The results demonstrate that the proposed control strategy optimizes the switching sequence and achieves fixed switching frequency control. It can effectively reduce switching losses and power losses, thereby lowering the harmonic content in the grid-connected side current. At the same time, the grid-connected current exhibits low harmonic content and minimal current ripple. Concurrently, the grid-connected current exhibits low harmonic content and minimal current ripple. Under dynamic conditions, it maintains high current tracking accuracy and demonstrates strong system robustness.

KEYWORDS: Photovoltaic grid-connected system; inverter; model predictive control; switching frequency; harmonic analysis

1 Introduction

We consider the broader framework to enrich the relevant context. As the era of electrification advances, power electronic devices such as variable frequency drives, inverters, and high-frequency switching power supplies have significantly impacted the operational quality of power systems. Inverter technology is widely applied in renewable energy generation, electric vehicle charging, industrial automation, and power systems. Its research background and significance are reflected in the following aspects: (1) Integration and utilization of renewable energy. (2) The proliferation of electric vehicles (EVs). (3) Enhancing energy efficiency and improving power quality. (4) Supporting industrial automation and smart manufacturing. The research and application of inverters are not only crucial for improving energy utilization efficiency and promoting environmental protection but also play a pivotal role in advancing new energy vehicles, smart grids, and industrial automation. Therefore, conducting research and promoting such technologies holds significant importance. With the advancement of the electrification era, power electronic devices such as frequency

converters, inverters and high-frequency switching power supplies have become indispensable parts of daily life, exerting a significant impact on the operational quality of the power system. Power electronic devices mainly operate through power switches. In most cases, they do not amplify power in a linear manner but are in a switching state. The two-level voltage source inverter (TL-VSI) is one of the core devices for energy conversion. Scholars at home and abroad are dedicated to researching ways to reduce the losses of inverters and improve their operating efficiency to meet strict control standards [1–3].

Among the control strategies of inverters, Model Predictive Control (MPC) is convenient for handling multivariable and nonlinear problems. Limited Control Set Model Predictive control (FCS-MPC) has been widely applied in many fields such as motor drive [4–6], power electronic converter [7,8] and power system [9] due to its significant advantages. The idea of combining MPC with three-phase voltage-type inverters was first proposed in reference [10], and it was applied to current predictive control. The research shows that the effect is good. Reference [11] proposed a control method for voltage source inverters. In each control cycle of the inverter, only one vector acts, which also leads to a relatively high harmonic content of the load current. Reference [12] improved the method in reference [11], proposing to use dual vectors for model prediction within one cycle. Although it overcomes the problem of large current pulsation in the traditional single-vector MPC strategy to a certain extent, the number of voltage vector searches is too many, which is not conducive to online optimization. At present, the inverter adopts the multi-vector model predictive control method, which can effectively reduce the current THD and improve the control effect [13,14]. References [15–19] further investigated low-loss operation control methods for inverters based on model predictive control methods. Reference [15] added an additional term for the number of power switch operations to the objective function of model predictive control. It achieved the objective function by designing corresponding weighting factors, thereby reducing the switching frequency and losses of the inverter. However, the weighting factor design in this method is overly complex. Reference [18] selects the voltage vector with the least number of switching operations of the power switch tubes of the inverter in the next control cycle based on the voltage vector acting on the inverter at the current moment, thereby reducing the switching frequency and decreasing the inverter's loss. According to the methods proposed in references [16–18], only one voltage vector is applied to the inverter within each control cycle, which results in a relatively large load current (total harmonic distortion, THD).

Regarding the issue of variable switching frequency, the literature [19,20] drew on the idea of Space Vector Pulse Width Modulation (SVPWM). And in each sampling period of the MPC, it always outputs three voltage vectors in the form of a switching sequence to act on the switching tubes. It achieved constant-frequency control. The literature [21] proposed an optimal switching sequence MPC strategy without weight coefficients, by adjusting the action time of the redundant voltage vectors to control the midpoint potential balance. However, due to the insufficient number of candidate vector sequences, the current tracking ability of the system may decline. The literature [22] effectively solved the problem of variable switching frequency by integrating the optimization decision-making ability of MPC with the fixed switching frequency characteristic of SVPWM. However, due to the addition of the modulation process, the overall system shows a trend of increased inertia. And the dynamic response performance is compromised. The literature [23–25] proposed various multi-vector MPC strategies applicable to permanent magnet synchronous motors. For example, the literature [25] applied the three-vector model predictive current control strategy to the permanent magnet synchronous motor. But there were problems of high switching frequency and complex calculation.

Consequently, the existing control methodologies fail to simultaneously achieve optimal performance across multiple criteria. Hardware-based approaches tend to increase system costs, and implementations of soft-switching control strategies are often complex. Space vector pulse-width modulation (SVPWM)

techniques can reduce inverter switching frequency and associated losses; however, their implementation is intricate, requiring substantial computational resources, which necessitates optimization in existing designs to mitigate computational burden. Adjusting the inverter control cycle can lower switching frequency but introduces challenges, as online modification affects steady-state current control, resulting in elevated total harmonic distortion (THD) of the current. In model predictive control (MPC), the simultaneous alteration of the cost function's weighting factors complicates the design process, and a comprehensive theoretical framework remains undeveloped. When only a single vector acts within each inverter control cycle, the inability of discrete basic vectors to approximate interpolated continuous reference vectors leads to significant waveform distortion, characterized by a high amplitude of harmonic voltage components. The inductive nature of the load further amplifies these distortions, culminating in current waveforms with pronounced high-order harmonic content and substantially increased harmonic distortions.

To this end, an improved control strategy for three-phase grid-connected inverters is proposed. The model predictive control algorithm is optimized within the dq0 coordinate system. An enhanced three-phase model predictive current control method integrating optimized switching sequences is introduced. This approach effectively addresses several issues: under conventional control strategies, the inverter's grid-connected current exhibits significant pulsations; instability in switching frequency results in a higher proportion of low-order harmonics in the grid-side current waveform; and at higher switching frequencies, problems such as increased switching losses adversely affecting the system's economic operation arise. Finally, the control performance of the proposed strategy is validated through experimental and simulation analyses.

2 The Working Principle and Mathematical Model of an Inverter

The topology of the three-phase two-level grid-connected inverter is shown in Fig. 1. Here, the DC regulated voltage is represented by U_{dc}, and e_a, e_b, and e_c represent the three-phase grid voltages. The filter inductors and capacitors of the three bridge arms of the inverter are taken as uniform values L and C.

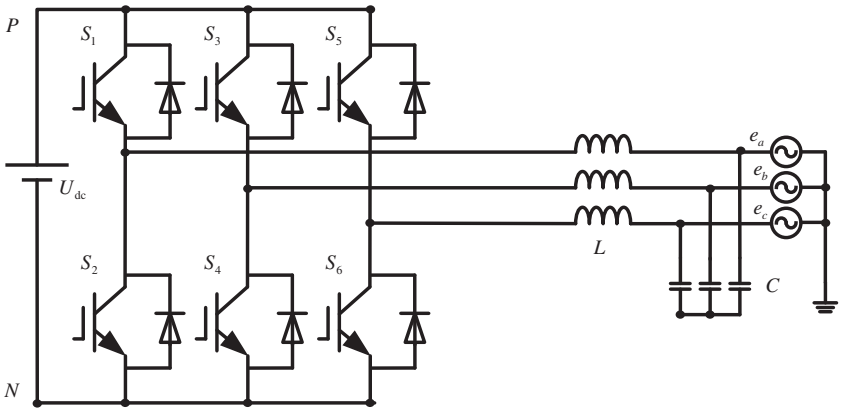

Figure 1: Topology of three-phase inverter

The three-bridge arm grid-connected inverter is composed of six IGBT power switch tubes. Each group of bridge arms has two switch tubes. During the commutation process, only one of the two switch tubes can be on at the same time; otherwise, a short circuit will occur. Switch states S_k ($k = 1, 2, \ldots, 6$), define the switch state as shown in Eq. (1).

$$S_x = \begin{cases} 1 \\ 0 \end{cases} (x = a, b, c) \tag{1}$$

The two-level three-bridge arm inverter has a total of $2^3 = 8$ switching state combinations: From 000 to 111, there are respectively 7 output voltage vectors, namely $V_0(0, 0, 0)$, $V_1(1, 0, 0)$, $V_2(1, 1, 0)$, $V_3(0, 1, 0)$, $V_4(0, 1, 1)$, $V_5(0, 0, 1)$, $V_6(1, 0, 1)$, and $V_7(1, 1, 1)$. Their corresponding relationships are shown in Fig. 2.

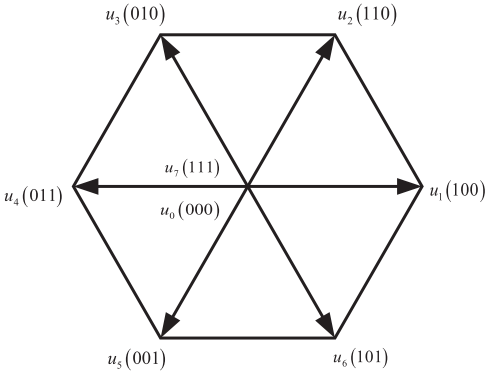

Figure 2: Inverter voltage vector figure

The switch signals in different states can be represented by space vectors as:

$$S = \frac{2}{3}\left(S_a + aS_b + a^2S_c\right) \tag{2}$$

among them $a = e^{j2\pi/3}$.

The voltage space vector of a three-phase symmetrical system can be calculated by Eq. (3):

$$\vec{U}_{ref} = \frac{2}{3}\left[U_{AN}(t) + U_{BN}(t)\, e^{j\frac{2\pi}{3}} + U_{CN}(t)\, e^{j\frac{4\pi}{3}}\right] \tag{3}$$

The schematic diagram of the three-phase two-level grid-connected inverter is shown in Fig. 1, then:

$$V_{abc} = L\frac{di_{abc}}{dt} + e_{abc} \tag{4}$$

The equivalent internal resistance of the inductor in its inverter is negligible.

The Clarke transformation of Eqs. (4) and (5) is carried out to obtain the mathematical models of each electrical quantity in the two-phase stationary αβ0 coordinate system.

$$C_{abc/\alpha\beta} = \frac{2}{3}\begin{bmatrix} 1 & -\frac{1}{2} & -\frac{1}{2} \\ 0 & -\frac{\sqrt{3}}{2} & -\frac{\sqrt{3}}{2} \end{bmatrix} \tag{5}$$

Eq. (4) is transformed by $C_{abc/\alpha\beta}$ to

$$\begin{cases} L\frac{di_\alpha}{dt} = V_\alpha - e_\alpha \\ L\frac{di_\beta}{dt} = V_\beta - e_\beta \end{cases} \tag{6}$$

among them: i_α, i_β, V_α, V_β, e_α and e_β are the components of each electrical quantity in the αβ0 coordinate system.

Perform the Park transformation on Eqs. (6) and (7) to transform it into the dq0 coordinate system.

$$C_{\alpha\beta/\mathrm{dq}} = \begin{bmatrix} \cos\theta & \sin\theta \\ -\sin\theta & \cos\theta \end{bmatrix} \tag{7}$$

Eq. (6) is transformed by $C_{\alpha\beta/\mathrm{dq}}$ to become

$$\begin{cases} L\dfrac{\mathrm{d}i_\mathrm{d}}{\mathrm{d}t} = V_\mathrm{d} - e_\mathrm{d} + \omega L i_\mathrm{q} \\ L\dfrac{\mathrm{d}i_\mathrm{q}}{\mathrm{d}t} = V_\mathrm{q} - e_\mathrm{q} - \omega L i_\mathrm{d} \end{cases} \tag{8}$$

among them, V_d, V_q, i_d, i_q, e_d and e_q respectively represent the direct and alternating axis components of the inverter's output voltage, grid-connected current, and grid-side voltage. The ω represents the angular frequency of rotation.

The predicted current value for the next moment is obtained by discretization using Euler's formula:

$$\begin{cases} i_\mathrm{d}(k+1) = i_\mathrm{d}(k) + \dfrac{T_\mathrm{s}}{L}\left[u_\mathrm{d}(k) - e_\mathrm{d}(k) + L\omega i_\mathrm{q}(k)\right] \\ i_\mathrm{q}(k+1) = i_\mathrm{q}(k) + \dfrac{T_\mathrm{s}}{L}\left[u_\mathrm{q}(k) - e_\mathrm{q}(k) + L\omega i_\mathrm{d}(k)\right] \end{cases} \tag{9}$$

Calculate the power value

$$\begin{bmatrix} p \\ q \end{bmatrix} = \begin{bmatrix} e_\mathrm{d} & e_\mathrm{q} \\ e_\mathrm{q} & -e_\mathrm{d} \end{bmatrix} \begin{bmatrix} i_\mathrm{d} \\ i_\mathrm{q} \end{bmatrix} \tag{10}$$

3 Inverter Control Strategy

3.1 *Three-Vector Model Predictive Current Control (TV-MPCC)*

Compared with the traditional single-vector and double-vector MPCC, TV-MPCC solves the limitation of the vector direction of the inverter output voltage under the first two methods. As shown in Fig. 2, Eq. (3) is represented on the complex plane. The eight space vectors U_0 to U_7 in the figure can be defined by Eq. (11):

$$\vec{U}_k = \begin{cases} \dfrac{2}{3}U_\mathrm{d} e^{j\frac{\pi}{3}(k-1)}, & k = 1, \ldots, 6 \\ 0, & k = 0, 7 \end{cases} \tag{11}$$

U_1 to U_6 represent six active vectors, and U_0 and U_7 represent two zero vectors. These eight vectors divide the plane in the figure into six sectors of the same size. In multi-vector control, they can be used to synthesize different output voltage vectors. Different vectors are used in different sectors for synthesis. For example, in the second sector, two adjacent vectors U_2 and U_3 as well as the zero vector U_0 are used to synthesize a new output vector. Similarly, the same method can be adopted in other sectors to synthesize the reference voltage vector and achieve better control performance.

3.2 *The Principle of TV-MPCC*

TV-MPCC method synthesizes a new voltage vector and takes it as the expected vector. It makes rational use of a zero vector and two adjacent effective vectors to generate it, which has the advantage of being able

to cover any amplitude and direction. The expected synthesis process of the voltage vector in six sectors is shown in Table 1 [21].

Table 1: Expected voltage vector synthesis

Sector	Zero vector	Effective vector	Expected vector
I	u_0 or u_7	u_1, u_2	u_{evvI}
II	u_0 or u_7	u_2, u_3	u_{evvII}
III	u_0 or u_7	u_3, u_4	u_{evvIII}
IV	u_0 or u_7	u_4, u_5	u_{evvIV}
V	u_0 or u_7	u_5, u_6	u_{evvV}
VI	u_0 or u_7	u_6, u_1	u_{evvVI}

Fig. 3 shows the system block diagram of TV-MPCC. The system adopts $i_{qref} = 0$. Firstly, three basic voltage vectors are selected. The action time of the vectors needs to be calculated using i_{dref} and i_{qref}. Then, a new voltage vector is generated. Finally, the optimal vector u_{out} is obtained through the optimization cost function. The S_a, S_b and S_c corresponding to u_{out} send signals to act on each bridge arm of the inverter.

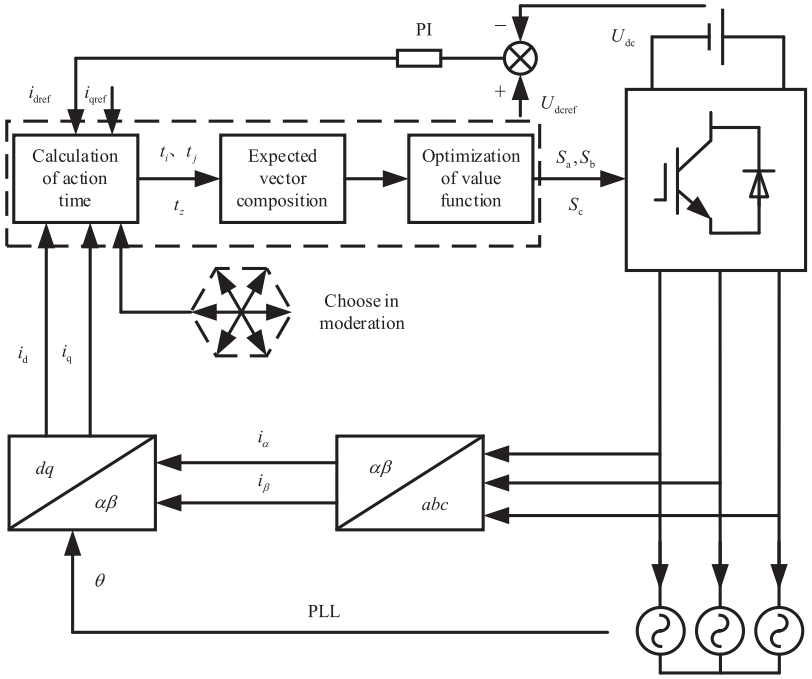

Figure 3: System block of TV-MPCC

3.3 Improve the Three-Vector Model for Predicting Current Control (ITV-MPCC)

3.3.1 Vector Action Time Calculation

In the ITV-MPCC strategy, the action times of the selected three basic vectors take into account the spot-free tracking of the AC and DC axis currents. Eqs. (12) and (17) respectively represent the calculation of the current slope.

$$S_{\mathrm{d}0} = \frac{\mathrm{d}i_{\mathrm{d}}}{\mathrm{d}t}\bigg|_{u_{\mathrm{d}}=0} = \frac{1}{L}\left[-e_{\mathrm{d}} + \omega L i_{\mathrm{q}}\right] \tag{12}$$

$$S_{\mathrm{q}0} = \frac{\mathrm{d}i_{\mathrm{q}}}{\mathrm{d}t}\bigg|_{u\mathrm{q}=0} = \frac{1}{L}\left[-e_{\mathrm{q}} - \omega L i_{\mathrm{d}}\right] \tag{13}$$

$$S_{\mathrm{d}i} = \frac{\mathrm{d}i_{\mathrm{d}}}{\mathrm{d}t}\bigg|_{u_{\mathrm{d}}=u_{\mathrm{d}i}} = S_{\mathrm{d}0} + \frac{u_{\mathrm{d}i}}{L} \tag{14}$$

$$S_{\mathrm{q}i} = \frac{\mathrm{d}i_{\mathrm{q}}}{\mathrm{d}t}\bigg|_{u_{\mathrm{q}}=u_{\mathrm{q}i}} = S_{\mathrm{q}0} + \frac{u_{\mathrm{q}i}}{L} \tag{15}$$

$$S_{\mathrm{d}j} = \frac{\mathrm{d}i_{\mathrm{d}}}{\mathrm{d}t}\bigg|_{u_{\mathrm{d}}=u_{\mathrm{d}j}} = S_{\mathrm{d}0} + \frac{u_{\mathrm{d}j}}{L} \tag{16}$$

$$S_{\mathrm{q}j} = \frac{\mathrm{d}i_{\mathrm{q}}}{\mathrm{d}t}\bigg|_{u_{\mathrm{q}}=u_{\mathrm{q}j}} = S_{\mathrm{q}0} + \frac{u_{\mathrm{d}j}}{L} \tag{17}$$

In Eqs. (14)–(17), $u_{di}, u_{qi}, u_{dj}, u_{qj}$ respectively represent the components of the vector u_i, u_j along the d and q axes.

Due to the adoption of the step-free control principle, the predicted value at the next moment during the sampling process is the given value. Therefore, the formula for the predicted current is shown in Eq. (18). In the formula, t_i, t_j, t_z represent the action times of the effective vector and the zero vector, respectively.

$$\begin{cases} i_{\mathrm{d}(k+1)} = i_{\mathrm{d}(k)} + s_{\mathrm{d}i}t_i + s_{\mathrm{d}j}t_j + s_{\mathrm{d}0}t_z = i_{\mathrm{dref}} \\ i_{\mathrm{q}(k+1)} = i_{\mathrm{q}(k)} + s_{\mathrm{q}i}t_i + s_{\mathrm{q}j}t_j + s_{\mathrm{q}0}t_z = i_{\mathrm{qref}} \end{cases} \tag{18}$$

The entire sampling period T_{s} is shown in Eq. (19).

$$T_{\mathrm{s}} = t_i + t_j + t_z \tag{19}$$

By combining Eqs. (12)–(19), we can obtain:

$$t_i = \frac{\left(i_{\mathrm{dref}} - i_{\mathrm{d}}(k)\right)\left(s_{\mathrm{q}j} - s_{\mathrm{q}0}\right)}{M} + \frac{\left(i_{\mathrm{qref}} - i_{\mathrm{q}}(k)\right)\left(s_{\mathrm{d}0} - s_{\mathrm{d}j}\right)}{M} + \frac{T_{\mathrm{s}}\left(s_{\mathrm{q}0}s_{\mathrm{d}j} - s_{\mathrm{q}j}s_{\mathrm{d}0}\right)}{M} \tag{20}$$

$$t_j = \frac{\left(i_{\mathrm{dref}} - i_{\mathrm{d}}(k)\right)\left(s_{\mathrm{q}0} - s_{\mathrm{q}i}\right)}{M} + \frac{\left(i_{\mathrm{qref}} - i_{\mathrm{q}}(k)\right)\left(s_{\mathrm{d}0} - s_{\mathrm{d}j}\right)}{M} + \frac{T_{\mathrm{s}}\left(s_{\mathrm{q}i}s_{\mathrm{d}0} - s_{\mathrm{q}0}s_{\mathrm{d}i}\right)}{M} \tag{21}$$

In the formula $M = s_{\mathrm{q}0}s_{\mathrm{d}j} + s_{\mathrm{q}i}s_{\mathrm{d}0} + s_{\mathrm{q}j}s_{\mathrm{d}i} - s_{\mathrm{q}i}s_{\mathrm{d}j} - s_{\mathrm{q}j}s_{\mathrm{d}0} - s_{\mathrm{q}0}s_{\mathrm{d}i}$

$$t_z = T_{\mathrm{s}} - t_i - t_j \tag{22}$$

After calculating the action times t_i, t_j, t_z of each vector, it is necessary to consider whether their values are within the sampling period T_{s}. If they are not within $0\sim T_{\mathrm{s}}$, the corresponding vector actions should be removed and classified according to specific circumstances:

(1) If t_i and t_j are within the sampling period of $0\sim T_{\mathrm{s}}$ and t_z is not within $0\sim T_{\mathrm{s}}$. Then the effective vectors u_i and u_j will act on one sampling period.

(2) Only one of t_i and t_j is within the sampling period of $0\sim T_{\mathrm{s}}$, and t_z is also within $0\sim T_{\mathrm{s}}$. Then, a valid vector from u_i or u_j, along with the zero vector, acts on one sampling period.

(3) If only one of t_i and t_j is within the sampling period of $0\sim T_s$, and t_z is not within $0\sim T_s$, then one of the effective vectors in u_i or u_j acts on one sampling period.

3.3.2 Expected Voltage Vector Synthesis

When synthesizing a new voltage vector, the selection of the effective vector follows the principle of proximity, taking two adjacent vectors within a sector. When choosing the zero vector, the premise of low switching loss should be followed. A new vector is synthesized in each sector according to this method, as shown in Fig. 4.

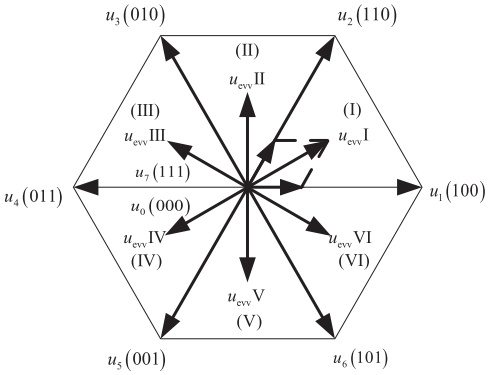

Figure 4: ITV-MPCC desired voltage vector synthesis

When calculating the synthesized voltage vectors u_{evv}I~u_{evv}VI, it is necessary to first calculate the voltage components of the synthesized voltage vectors on the AC and DC axes, respectively, as shown in Eqs. (23) and (24).

$$u_d = \frac{t_i}{T_s}u_{di} + \frac{t_j}{T_s}u_{dj} \tag{23}$$

$$u_q = \frac{t_i}{T_s}u_{qi} + \frac{t_j}{T_s}u_{qj} \tag{24}$$

Substitute the calculated voltage component into Eq. (10) to calculate the predicted value of the current. The cost function is constructed for optimization using the calculated current prediction value and reference value, as shown in Eq. (25). Select the u_{out} that can minimize g to act on the inverter.

$$g = \left|i_{qref} - i_q\left(k+1\right)\right| + \left|i_{dref} - i_d\left(k+1\right)\right| \tag{25}$$

4 Optimize the Switch Sequence

The fluctuation of the switching frequency leads to a relatively high content of low-order harmonics in the network-side current waveform. If no additional control measures are taken, it will affect the system's operational performance. At the same time, the switching frequency of MPC may fluctuate. When the frequency is relatively high, the switching loss of the system at this time is relatively unfavorable for the economic operation of the system in practice. In principle, there are two schemes to reduce the switching loss of the system: one is to minimize the total number of changes in the switching state of the system throughout its operation; The second is to adopt a control strategy to keep the system's switching frequency always at a low and fixed value. This chapter adopts a new control scheme, effectively combining these two schemes to significantly reduce the switching loss of the system. According to the operating principle, let its switching

state be X = [S_1 S_5 S_4 S_2 S_6 S_3], where S_1 to S_6 take 1 to indicate that the switch is on or 0 to indicate that the switch tube is off.

Taking time k X = [100001] as an example, all possible switch states of the system at the next time $k + 1$ can be written. The number of switch switches may be 0, 2, or 4 times. To reduce system losses, the number of switch switches should be as few as 0 and 2 times as possible, and avoid 4 times. Then, the optimal switch sequence for the next moment of X is fixed to be selected from X_1, X_2, X_6, X_7, and X_9. Similarly, the optimal switch sequence corresponding to the next moment for all switch states can be sorted out.

As shown in Fig. 5, the following details the switching conditions and frequencies. Suppose the switch state of the inverter at time k is X = [100001]. According to the preset switch representation rule. The digit 1 indicates that the switch is conducting, and the digit 0 indicates that the switch is turned off. Therefore, all possible switch states at the next time $k + 1$ can be represented as the following situations. X_1 = [100001], X_2 = [010001], X_3 = [010100], X_4 = [001101], X_5 = [001010], X_6 = [100010], X_7 = [100100], X_8 = [010010], X_9 = [001001]. Here, X_1 has changed the switch 0 times, X_2 has changed the switch 2 times, X_3 has changed the switch 4 times, X_4 has changed the switch 4 times, X_5 has changed the switch 4 times, X_6 has changed the switch 2 times, X_7 has changed the switch 2 times, X_8 has changed the switch 4 times, and X_9 has changed the switch 2 times. To reduce system losses, the number of switch switching times should be as 0 and 2 as much as possible, and avoid 4 times. Therefore, the optimal switch sequence of X at the next time is fixed to be selected from X_1, X_2, X_6, X_7, and X_9. This way, the system's switching frequency can always remain at a low fixed value, and the total number of switch state changes throughout the entire operation process of the system is minimized.

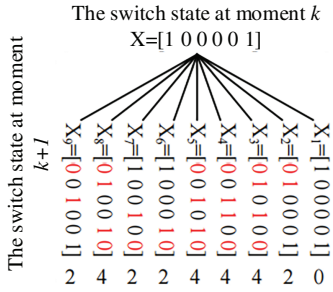

Figure 5: Diagram of the changes and frequency of switch switching

The above control concept can be realized by adding a switching frequency constraint term to the cost function of ITV-MPCC, as shown in Eq. (26). The number of switch switches can be obtained by subtracting the switch states at the previous and subsequent times:

$$F = g + \sum_{j=1}^{6} |X_{k+1} - X_k| \tag{26}$$

Through optimization, the switching state corresponding to the fewest switching times of the switching function can be obtained and applied to the inverter, achieving fixed switching frequency control. It has solved the problem of high harmonic content of grid-side current caused by the unstable frequency of traditional MPC, and at the same time, the optimized control algorithm has reduced the computational load. Adopting this approach greatly reduces the computational pressure, enabling the system to respond more quickly.

By using six-sector modulation in the a–β coordinate system, a signal with a constant switching frequency for driving the power switch tube can be obtained. The 6-sector vector modulation voltage vector and the spatial distribution of the sectors are shown in Fig. 6.

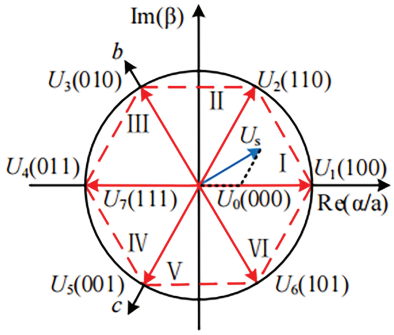

Figure 6: Schematic diagram of voltage vector selection

5 Simulation and Experimental Verification

To verify the correctness and effectiveness of the proposed scheme, we conducted simulations and experimental validations. The parameters are shown in Table 2.

The parameters set are as shown in the following table.

Table 2: Parameter settings

Parameter	Numerical value	Parameter	Numerical value
DC side voltage	650 V	Filter capacitor	0.5 μF
Frequency	50 HZ	Sampling frequency	10 kHZ
Line resistance	0.1 Ω		

5.1 Current Tracking Comparison

Fig. 7 shows the experimental waveform of the traditional MPC. Although the sine effect of the grid-connected voltage and current is good, the three-phase current waveform has certain burrs and the current distortion is relatively large, as shown in Fig. 7a. Taking the current of phase a as an example, spectral analysis was conducted on it in the simulation software, as shown in Fig. 7b. According to the analysis results, its THD is 4.03%, which is less than 5%. Although it meets the grid connection requirements, its waveform quality is poor.

The simulation results of the proposed control strategy are shown in Fig. 8. By comparing with the traditional MPCC, it can be seen that the proposed control strategy has no significant impact on the grid-connected voltage, which fluctuates sinusoidal within ±311 V, as shown in Fig. 8a. The grid-connected current responds rapidly to a sinusoidal waveform. The spectral analysis of the A-phase current under the proposed control strategy is shown in Fig. 8b. Compared with traditional MPCC, the quality of the current waveform has been greatly improved, with THD dropping from 4.03% to 0.89%, and the distortion rate of grid-connected current has been significantly reduced.

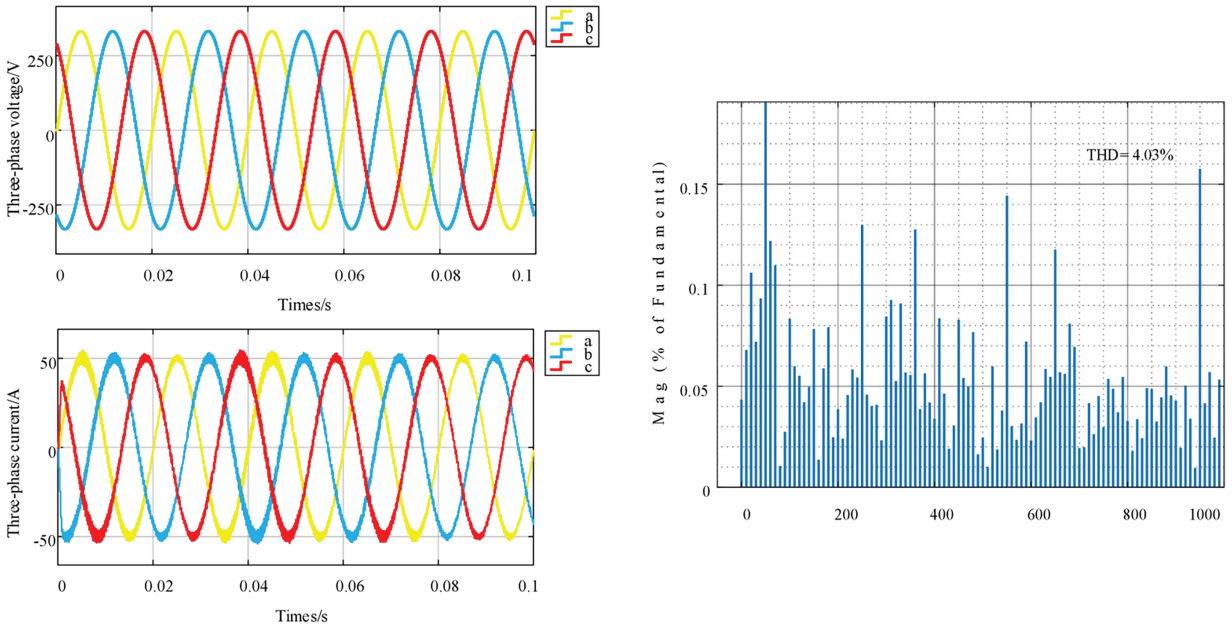

Figure 7: Traditional MPCC

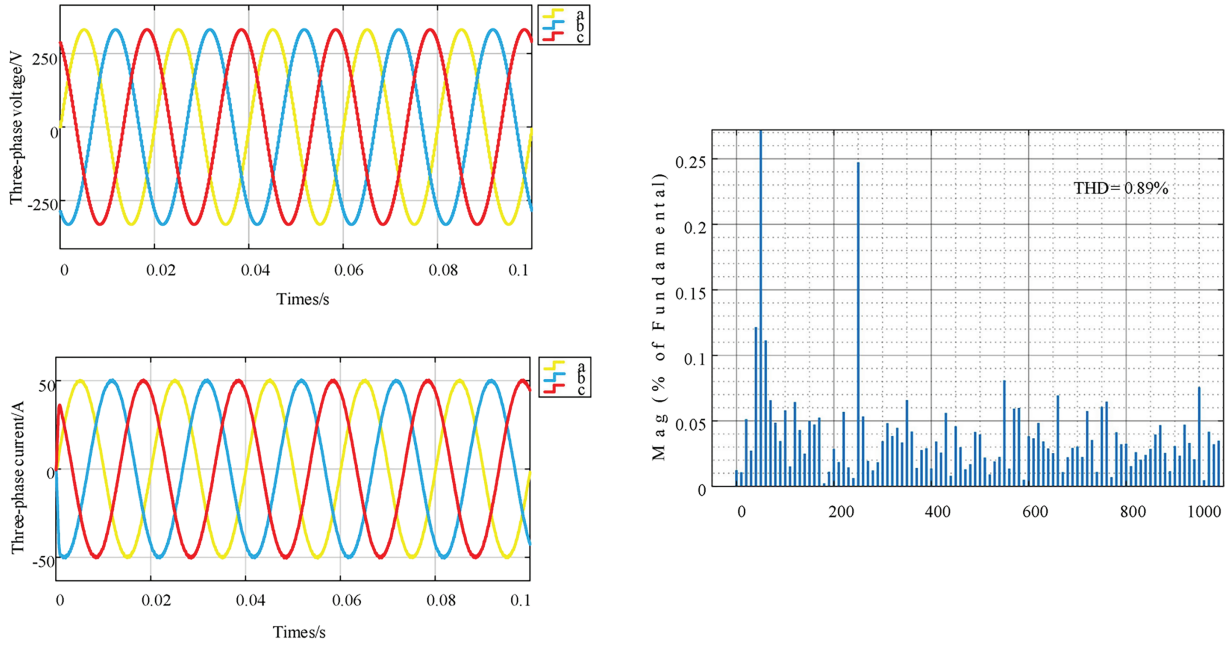

Figure 8: The proposed control strategy

Fig. 9 shows the current waveforms of i_d and i_q. Fig. 9a shows that the traditional MPCC control is adopted, which has a poor current control effect. The dq axis components all have large pulsations. Fig. 9b shows the proposed control strategy, which performs beat free control on both axis components. The current ripple rate is significantly reduced compared to the control. The current fluctuations of i_d and i_q were reduced by 90% and 86%, respectively. The current pulsation of the two axis components can be ignored, which is the same as the simulation result of the network measurement current.

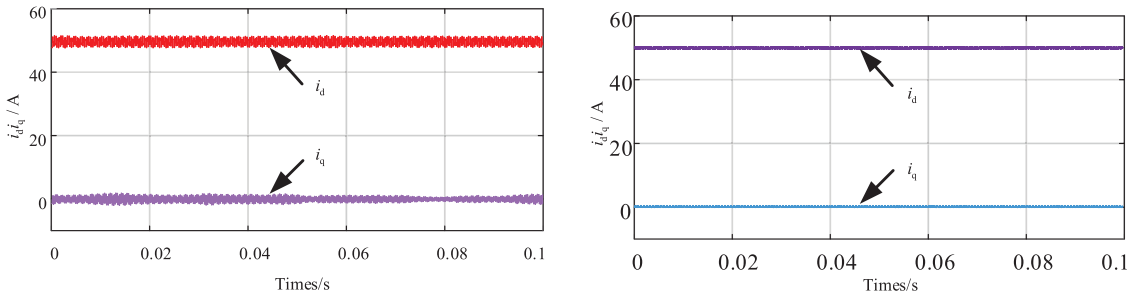

(a) traditional MPCC (b) the proposed control strategy

Figure 9: dq-axis current waveform

5.2 Dynamic Performance Analysis

Fig. 10 shows the current tracking situation of the network measurement proposed in this paper under dynamic conditions. As shown in Fig. 10a, it is the dynamic response result of the A-phase grid-connected current on the grid side. The sinusoidal degree of the output waveform is very good, and the sideband harmonic content of the proposed control strategy slightly increases. The main reason is that the output current of the inverter is relatively small. When the output current is increased, it can be effectively improved. It can be quickly tracked and is almost in the same frequency and phase as the grid-connected voltage. And when the output current increases, the current stabilizes within 0.008 s. Fig. 10b shows the result of i_d tracking the reference value i_{dref}. The predicted value basically coincides with the reference value, indicating a rapid response and maintaining stability during operation.

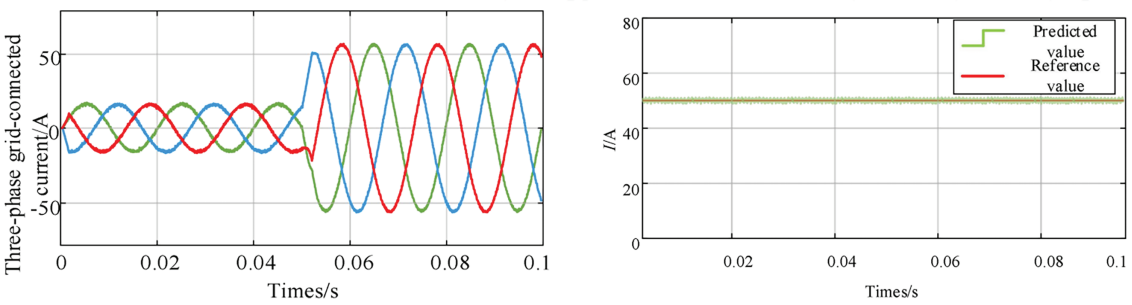

Figure 10: The proposed control strategy is current tracking

5.3 Comparison of Switching Frequencies

To verify the effectiveness of the proposed control strategy in reducing the switching frequency and power loss. The equivalent switching frequency and power loss are defined as shown in Eqs. (27) and (28), respectively.

$$f_{avgsw} = \sum_{i=1,3,5} \frac{f_{swi}}{3} \tag{27}$$

In the formula, f_{swi} represents the switching frequency of the power switch tube within one fundamental period.

$$\Delta loss = \frac{loss_C - loss_D}{loss_C} \times 100\% \tag{28}$$

In the formula, $loss_c$ represents the power loss generated by the traditional MPCC, and $loss_D$ is the loss produced under the proposed strategy.

Fig. 11 shows the comparison results of the equivalent switching frequency and power loss between the three-phase grid-connected inverter and the traditional MPCC under the proposed control strategy. The proposed strategy fixes the switching frequency by optimizing the voltage vector selection and the switching sequence, thereby reducing the number of switching times of the switching tube at high currents. From Fig. 11a, it can be analyzed that the equivalent switching frequency of the proposed control strategy has been reduced by approximately 45.7%. Fig. 11b indicates that the loss has decreased by approximately 23.6%. It effectively reduces the power loss of the inverter and improves the grid-connected operation efficiency of the system.

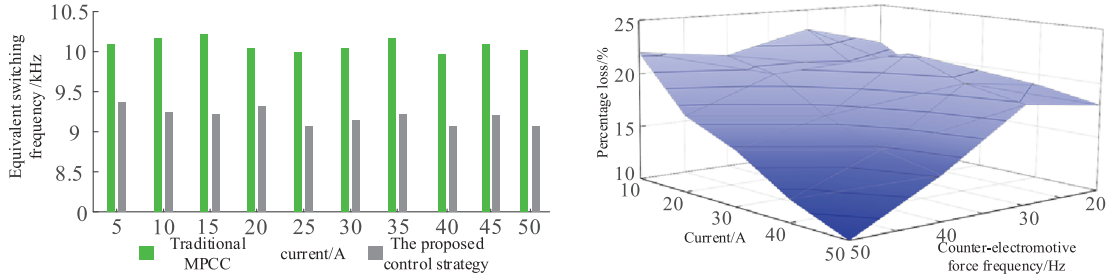

(a) comparison of equivalent switching frequencies (b) percentage reduction in loss

Figure 11: Comparison of switching frequency and power loss

6 Conclusion

This paper proposes an improved three-vector model predictive current control method for three-phase grid-connected photovoltaic inverters, incorporating an optimized switching sequence. The approach effectively addresses several challenges: under conventional control strategies, inverter grid-connected current ripple is significant; variable switching frequencies result in an increased proportion of low-order harmonics in the grid current waveform; and at higher system switching frequencies, practical issues such as increased switching losses emerge, adversely affecting economic operation.

(1) The proposed control strategy reduced the grid-connected current THD from 4.03% to 0.89%, significantly decreasing the current distortion level. The current ripple in both the direct (i_d) and quadrature (i_q) axes decreased by 90% and 86%, respectively. Accordingly, the system's steady-state performance was markedly enhanced. The control demonstrates robust stability and superior dynamic response.

(2) The proposed control strategy optimizes switching sequences to achieve fixed switching frequency operation. This approach reduces the harmonic content of the grid-side current, effectively diminishes switching and power losses. The effective switching frequency and associated losses are decreased by approximately 45.7% and 23.6%, respectively. Additionally, the optimized control algorithm reduces computational complexity, thereby enhancing the inverter's operational efficiency.

(3) Under dynamic conditions, an increase in output current significantly enhances the waveform quality. Additionally, as the output current rises, the current stabilizes within 0.008 s, reaching the desired output level. This system exhibits excellent dynamic performance, improving computational efficiency and facilitating more straightforward program development and practical implementation.

Acknowledgement: Not applicable.

Funding Statement: This work was supported in part by the National Natural Science Foundation of China (No. 52467008), Gansu Provincial Department of Education Youth Doctoral Support Project (2024QB-051) and Innovation Project for Young Science and Technology Talents in Lanzhou City (2023-QN-121).

Author Contributions: The authors confirm contribution to the paper as follows: study conception and design: Dan Li, Hongsheng Su; data collection: Yuwei Du; analysis and interpretation of results: Dan Li, Hongsheng Su, Yuwei Du; draft manuscript preparation: Dan Li. All authors reviewed and approved the final version of the manuscript.

Availability of Data and Materials: All data generated or analyzed during this study are included in this published article.

Ethics Approval: Not applicable.

Conflicts of Interest: The authors declare no conflicts of interest to report.

References

1. Xu L, Xia L, Wang S, Zheng J, Li S, Zhang Q. Research on building energy system management system based on new power system under carbon peaking and carbon neutrality goals. In: Proceedings of the 2024 IEEE 8th Conference on Energy Internet and Energy System Integration (EI2); 2024 Nov 29–Dec 2; Shenyang, China. p. 589–93. doi:10.1109/EI264398.2024.10991560.
2. Makanju TD, Hasan AN, Famoriji OJ, Shongwe T. An intelligent technique for coordination and control of PV energy and voltage-regulating devices in distribution networks under uncertainties. Energies. 2025;18(13):3481. doi:10.3390/en18133481.
3. Benagri I, Haidi T, Derri M, Mellouli EM, Zahraoui Y, Cherrabi M. Comparison of the fundamental topologies of multilevel inverters with two-level inverters for electric vehicle applications: a synthesis. In: Proceedings of the 2025 5th International Conference on Innovative Research in Applied Science Engineering and Technology (IRASET); 2025 May 15–16; Fez, Morocco. p. 1–6. doi:10.1109/IRASET64571.2025.11007983.
4. Wu W, Qiu L, Rodriguez J, Liu X, Ma J, Fang Y. Data-driven finite control-set model predictive control for modular multilevel converter. IEEE J Emerg Sel Top Power Electron. 2023;11(1):523–31. doi:10.1109/JESTPE.2022.3207454.
5. Feng Q, Zhang M, Xu Y, Zhang C, Chen D, Yuan X. A multi-vector modulated model predictive control based on coordinated control strategy of a photovoltaic-storage three-port DC-DC converter. Energies. 2025;18(12):3208. doi:10.3390/en18123208.
6. Yan L, Wang F. Observer-predictor-based predictive torque control of induction machine for robustness improvement. IEEE Trans Power Electron. 2021;36(8):9477–86. doi:10.1109/TPEL.2021.3050825.
7. Bonaldo J, Duan B, Rivera M, Ling KV, Fantin C, Wheeler P. Comprehensive performance assessment of conventional and sequential predictive control for grid-tied NPC inverters: a hardware-in-the-loop study. Energies. 2025;18(12):3132. doi:10.3390/en18123132.
8. Zhou Z, Wang J, Zhang S. Speed synchronization control strategy of dual-motor system with explicit model predictive control. IEEE J Emerg Sel Top Power Electron. 2024;12(3):2787–98. doi:10.1109/JESTPE.2024.3390999.
9. Sheikhi Jouybary H, Arab Khaburi D, El Hajjaji A, Mpanda Mabwe A. Optimal sliding mode control of modular multilevel converters considering control input constraints. Energies. 2025;18(11):2757. doi:10.3390/en18112757.
10. Rodríguez J, Pontt J, Silva C, Salgado M, Rees S, Ammann U, et al. Predictive control of three-phase inverter. Electron Lett. 2004;40(9):561–3. doi:10.1049/el:20040367.
11. Zhou H, Li H, Xiang X, Yuan B, Zhou T, Li W. Model predictive control algorithm of dual three-phase motor considering global single vector. In: Proceedings of the 2022 25th International Conference on Electrical Machines and Systems (ICEMS); 2022 Nov 29–Dec 2; Chiang Mai, Thailand. p. 1–6. doi:10.1109/ICEMS56177.2022.9983256.
12. Fu D, Zhao X, Zhu J. A novel robust super-twisting nonsingular terminal sliding mode controller for permanent magnet linear synchronous motors. IEEE Trans Power Electron. 2022;37(3):2936–45. doi:10.1109/TPEL.2021.3119029.

13. Chen Z, Dawara AA, Zhang X, Zhang H, Liu C, Luo G. Adaptive sliding mode observer-based sensorless control for SPMSM employing a dual-PLL. IEEE Trans Transp Electrific. 2022;8(1):1267–77. doi:10.1109/tte.2021.3112123.
14. Zhang Y, Bai Y, Yang H. A universal multiple-vector-based model predictive control of induction motor drives. IEEE Trans Power Electron. 2018;33(8):6957–69. doi:10.1109/TPEL.2017.2754324.
15. Danyali S, Aghaei O, Shirkhani M, Aazami R, Tavoosi J, Mohammadzadeh A, et al. A new model predictive control method for buck-boost inverter-based photovoltaic systems. Sustainability. 2022;14(18):11731. doi:10.3390/su141811731.
16. Kwak S, Park JC. Switching strategy based on model predictive control of VSI to obtain high efficiency and balanced loss distribution. IEEE Trans Power Electron. 2014;29(9):4551–67. doi:10.1109/TPEL.2013.2286407.
17. Kwak S, Park JC. Predictive control method with future zero-sequence voltage to reduce switching losses in three-phase voltage source inverters. IEEE Trans Power Electron. 2015;30(3):1558–66. doi:10.1109/TPEL.2014.2304719.
18. Yousefi-Talouki A, Zalzar S, Pouresmaeil E. Direct power control of matrix converter-fed DFIG with fixed switching frequency. Sustainability. 2019;11(9):2604. doi:10.3390/su11092604.
19. Yan Q, Chen H, Zhao T, Yuan X, He J, Xu H, et al. Optimization of the symmetrical SVPWM for three-level T-type inverters with unbalanced and oscillated neutral-point voltages. IEEE Trans Ind Electron. 2024;71(4):4026–37. doi:10.1109/TIE.2023.3279521.
20. Cui K, Wang C, Zhou M, Sun S. Comprehensive investigation of space-vector PWM including novel switching sequences for dual three-phase motor drives. IEEE Trans Transp Electrif. 2023;9(1):1350–62. doi:10.1109/TTE.2022.3198718.
21. Chen S, Yang Y, Fan M, Chen R, Xiao Y, Wen H, et al. A simplified optimal switching sequence model predictive control without weighting coefficients for T-type single-phase three-level inverters. IEEE Trans Transp Electrific. 2024;10(3):5936–46. doi:10.1109/tte.2023.3323460.
22. Wang YZ, Huang S, Liao W, Zhang Y, Huang SD. IPMSM model predictive current control method based on a vector modulation method. Nov Virtual Trans China Electrotech Soc. 2024;39(8):2422–33. (In Chinese). doi:10.1109/tte.2023.3281742.
23. Chen R, Shu HP, Zhai KM. Low-complexity three-vector model predictive current contml with fixed switching for PMSM. Proc CSEE. 2024;44(9):3710–22. (In Chinese).
24. Yang Y, Wen H, Fan M, He L, Xie M, Chen R, et al. Multiple-voltage-vector model predictive control with reduced complexity for multilevel inverters. IEEE Trans Transp Electrific. 2020;6(1):105–17. doi:10.1109/tte.2020.2973045.
25. Lin J, Zhang S, Zhou L, Zha Y, Sun J. Improved sliding mode control of permanent magnet synchronous linear motor based on model-assisted linear extended state observer. IEEE Access. 2022;10(7):70815–24. doi:10.1109/ACCESS.2022.3186984.